coatings

Article

Effect of Rare Earth Y on the Microstructure, Mechanical Properties and Friction of Sn-Babbitt Alloy

Xiaoyan Ren [1,*], Yuan Chang [2], Shengsheng Chen [3], Ningning Chen [2], Zhenghua Shi [2], Yougui Zhang [2], Huimin Chen [2], Zhiming Guo [1], Jinzhi Hu [1], Guowei Zhang [2,*] and Hong Xu [2,*]

1 Department of Mechanical Engineering, Taiyuan Institute of Technology, Taiyuan 030008, China; guozhiming0602@163.com (Z.G.); 13099087838@163.com (J.H.)
2 School of Materials Science and Engineering, North University of China, Taiyuan 030051, China; cy2053557877@163.com (Y.C.); cnn18834145071@163.com (N.C.); szh1564067917@163.com (Z.S.); z18234902741@163.com (Y.Z.); 15536701731@163.com (H.C.)
3 State Key Laboratory of Solid Lubrication, Lanzhou Institute of Chemical Physics, Chinese Academy of Sciences, Lanzhou 730030, China; chenshengsheng@licp.cas.cn
* Correspondence: renxiaoyan03@126.com (X.R.); 20030358@nuc.edu.cn (G.Z.); xuhong@nuc.edu.cn (H.X.)

Abstract: Babbitt alloy is a bearing material with excellent properties, including good anti-friction wear resistance, embeddedness, corrosion, and compliance, as well as sufficient bearing capacity. However, with the development of engines to have high speed and heavy load, the use of Babbitt alloy as a bearing material exposes its weaknesses of low bearing capacity, insufficient fatigue strength and a sharp decline in mechanical properties with an increase in working temperature. Therefore, its application scope is gradually narrowed and subject to certain limitations. Improving the tensile strength and wear resistance of tin-based Babbitt alloy is of great significance to expanding its application. In this study, tin-based Babbitt alloy was taken as the main research object; the particle size, microstructure, mechanical properties, and friction were systematically studied after the single addition of Y-Cu composite in tin-based Babbitt alloy liquid. The wear performance and the strengthening, toughening and wear mechanisms of tin-based Babbitt alloy were investigated under the action of Y in order to prepare a high-performance tin-based Babbitt alloy for bimetallic bearing. It was found that when rare-earth Y was added to the Babbitt alloy body, the wear properties were greatly improved.

Keywords: tin base Babbitt alloy; microstructure; grain refinement; mechanical properties; Abrasion resistance

Citation: Ren, X.; Chang, Y.; Chen, S.; Chen, N.; Shi, Z.; Zhang, Y.; Chen, H.; Guo, Z.; Hu, J.; Zhang, G.; et al. Effect of Rare Earth Y on the Microstructure, Mechanical Properties and Friction of Sn-Babbitt Alloy. *Coatings* **2024**, *14*, 1325. https://doi.org/10.3390/coatings14101325

Academic Editor: Cecilia Bartuli

Received: 30 July 2024
Revised: 1 October 2024
Accepted: 9 October 2024
Published: 16 October 2024

1. Introduction

Tin-based Babbitt alloy mainly consists of a tin-based solid solution as the α soft matrix phase, a dispersed hard β phase and a dispersed Cu_6Sn_5 phase. Due to the characteristics of a soft matrix inlaid with hard particles, it has good wear resistance, corrosion resistance and embedding ability. Therefore, Babbitt alloy is commonly used as a plain-bearing material in large steam turbines, compressors, ships and other industrial fields. However, in a variety of heavy-duty, high-speed and low-speed plain bearings, it is very common for Babbitt materials to burn and fail due to the instability of the lubricating oil film [1–4]. The characteristics of high thermal conductivity, good embeddability and flexible conformability of Babbitt alloys [5–8], along with their anti-friction property [9], have been well-recognized, with these alloys being utilized as bearing pads and/or bearing sleeves in many types of bearing components.

In actual work, when the shaft rotates at a high speed, the surface of the bearing bush bears a certain periodic alternating load, especially when starting and stopping. The high content of C and O in the oil film results in the gradual formation of carbon deposits on the surface of the bearing bush, and the parallel degree of the bearing bush's thrust disk becomes worse. The contact between the shaft journal becomes uneven, and the oil film is destroyed. On one hand, this causes serious friction between the Babbitt alloy and the shaft journal, and the accumulation of friction heat causes the surface temperature to rise. When the temperature reaches the melting point of the matrix, the matrix begins to soften or even appears in a molten state. Under the action of friction, the surface of the matrix can produce a plastic flow, forming traces of macroscopic friction and resulting in the Babbitt alloy having soft hardness and cracking or even spalling. On the other hand, the uneven contact between the bearing bush and the journal leads to the blocking of the oil film on the surface of the bearing bush, the deposition of impurity elements on the surface of the bearing bush during operation, the electrochemical corrosion of the Babbitt alloy matrix and the formation of an electric corrosion pit [10–13]. Therefore, it is crucial to improve the wear resistance of Babbitt alloy.

Recent research on bearing Babbitt alloy has mainly focused on the manufacturing process and the composition improvement of Babbitt alloy. For instance, in order to obtain Babbitt alloy materials with better performance, Tasgin et al. [14] added a variety of boron compounds into Babbitt alloy and studied its metallographic organization and wear performance. Paulo et al. [15] compared the spraying and pouring processes of Babbitt alloy, and the results showed that the Babbitt alloy obtained by thermal spraying has higher porosity and a lower wear rate. Nascimento et al. [16] adopted the high-speed oxygen-fuel (HVOF) spraying process, and good distribution of the alloy phase was obtained. At Shiraz University, Arab, SM [17] innovatively used the friction stir processing (FSP) method to prepare Babbitt alloy materials with fine grains, high microhardness, and high friction resistance. At Sun Moon University, Amanov, A. et al. [18] used the ultrasonic nanocrystal line surface modification technology to improve the friction and wear performance of Babbitt alloy in the oil film bearing of the cone crusher.

Other scholars have carried out research on the friction and wear properties of Babbitt alloy. For example, Zhang et al. [19] used the pin-on-disk friction testing machine and numerical simulation to analyze the lubrication performance and mechanism of the texture of Babbitt alloy and studied the tribological performance of the surface texture to improve the mixed friction of oil film bearings. Zhang D. [20] studied the dry friction properties of polyurethane coating and tin-based Babbitt alloy. Ji X. [21] found that, under dry friction conditions, the sliding speed has an influence on the friction and wear of Babbitt alloy. Liu et al. studied the sliding tribological behavior of tin-based Babbitt alloy under the condition of seawater lubrication [22,23].

K. Sürül et al. [24] studied the bonding strength of the Babbitt alloy Sn-12Sb-6Cu-1.8Bi. This new high-performance Babbitt alloy contained 1.8 wt.% bismuth as a solid solution strengthener, which produced very good bonding strengths in all the investigated tin-based Babbitt alloy materials.

Abioye, T. E. et al. [25] studied the effects of SiC addition on the microstructure, compressive strength and wear resistance of Sn-Sb-Cu alloy developed via powder metallurgy (PM). The microstructure showed the presence of a Sn-rich matrix, a randomly dispersed Cu phase in the matrix, and the formation of a SnSb hard phase along the grain boundaries. The ratio of the SnSb:Sn phases could be increased by increasing the addition of SiC. The hardness, compressive strength and wear resistance of the Sn-Sb-Cu alloy were found to increase with an increase in the SiC composition, with an improvement of ~43% in hardness, ~55% in compressive strength and ~80% in wear resistance.

Zh. Cheng et al. [26] researched the properties of tin-based Babbitt alloy B83, which was designed by adding trace Ag (1%, 3%) and graphite (1%) into molten B83 via metallographic control in order to improve the properties of the Babbitt layer, meet the requirements of rotating machinery, and further promote the development of high-end sliding bearings. The research results indicate that adding trace Ag and graphite into B83 promoted refinement and uniform distribution of the hard particles of B83, which is beneficial to improving the mechanical and tribological properties of B83. In particular, adding 1% Ag remarkably improved the high-temperature hardness, while adding trace graphite made the Babbitt alloy more stable with a certain self-lubrication and friction coefficient. Both the mechanical and tribological properties of B83 improved remarkably with the addition of 1% Ag, which becomes more suitable for the bearing of high-speed motorized spindles and micro-gas turbines.

Zh. Cheng et al. [27] prepared Babbitt alloy SnSb12Cu7.5Ni0.9-X (Ag, Co, Cr) via induction smelting. The results showed that, with the addition of 1% Ag, Co and Cr, the square SnSb phase in the SnSb12Cu7.5Ni0.9 alloy structure was refined and slightly passivated. In addition, the granular η phase (Cu_6Sn_5) changed from a slender strip to worm-like. With the addition of 1 wt.% Ag, Co and Cr, the bonding strength of the Babbitt alloy/steel matrix was improved. The highest bonding strength was 51.9 MPa when 1 wt.% Co was added, which was 13% higher than that of the matrix.

GONG Liukui et al. [28] fabricated Sn-58Bi-Y alloys with different Y contents (0.0%, 0.1%, 0.2%, 0.3%, 0.4% and 0.5%) in a vacuum furnace under a nitrogen atmosphere. The results showed that the Sn-Bi microstructure was refined. The rare-earth Y was evenly distributed in the Bi-rich phase. The melting points and melting ranges were less affected by the addition of the Y content. The hardness of Sn-58Bi alloys increased to the maximum value of 24.18 HV when the content of Y was 0.4%. Therefore, Y can promote the reaction of Sn-58Bi solder with Cu during welding and form a Cu_6Sn_5 intermetallic compound.

As can be seen from the above literature, most researchers' optimization of Babbitt alloy materials has mainly focused on Ag, Co, Cr and so on. Due to the wide application of rare-earth Y in other materials, this study mainly investigated the influence of rare-earth Y on the organization and performance of ZSnSb11Cu6 alloy in order to improve the friction wear properties of this Babbitt alloy.

2. Experimental Procedure

2.1. Preparation of As-Casted ZSnSb11Cu6 Alloy

The raw material used in this experiment was tin-based Babbitt alloy with the grade of ZSnSb11Cu6. To improve its properties, the effects of Y on the microstructure and mechanical properties of the ZSnSb11Cu6 alloy were studied by adding different contents of the trace element Y. Referring to the previously studied effects of rare-earth Y and La on the organization and properties of copper alloys [29,30], the chemical composition of this tin-based Babbitt alloy is shown in Table 1. This alloy is the basis for the pre-smelting ingredients.

Table 1. Chemical composition of ZSnSb11Cu6 alloy used for smelting (wt.%).

No.	Sn	Sb	Cu	Y
1	Bal.	11	6	0
2	Bal.	11	6	0.04
3	Bal.	11	6	0.08
4	Bal.	11	6	0.12
5	Bal.	11	6	0.16

2.2. Experimental Method

The experiment was conducted via melting in a well-resistance furnace and using a graphite crucible. The 12# graphite crucible was baked and reinforced in the furnace before use (600 °C for 1 h, followed by 400 °C for 1 h and 200 °C for 1 h). Because of the high melting point of Cu-Y alloy, it was ground into fine particles before use (the smaller the particles, the better) and wrapped with copper foil for reserve. When smelting, the crucible was first placed in the furnace at 250 °C for preheating. The melting furnace's temperature was gradually raised to 430 °C, and a certain ratio of ZSnSb11Cu6 alloy and Cu-Y alloy particles was placed in the preheated crucible and then into the melting furnace. The temperature was adjusted to ensure that all ZSnSb11Cu6 alloy and yttrium copper particles were melted; the liquid was stirred, and its temperature was measured with a graphite rod preheated to about 300 °C to ensure that the liquid was poured at 430 °C. The mold was opened after 20 min.

The mechanical tensile test was carried out using a WDW-20/30 universal electronic mechanical testing machine; the loading tensile rate was 2.4 mm/min, and the gauge length of the tensile specimen was 40 mm. The Brinell hardness was measured using a HB-300B Brinell hardness tester; each sample was measured 5 times, and the average value was taken at the end.

After smelting, the samples were taken to the same location for analysis. The friction and wear properties of the samples were tested using an MRH-3 ring-on-block friction tester. The standard sample size was 12.32 mm × 12.32 mm × 19.05 mm cuboid. After the friction test, the microstructure and morphology of the worn surface were observed using a metallographic microscope (AXIO Scope.A1, ZEISS, Jena, Germany), and the etching solution was a 4% nitric acid alcohol solution. The morphology of the Babbitt alloy was observed using thermal field-emission scanning electron microscope (SEM, Sigma 300, ZEISS, Jena, Germany), whose built-in energy spectrometer function was employed to perform energy spectrum analysis on the composition of the alloy structure and the precipitated phase. The Setaram Labsys synchronous thermal analyzer was used to detect and analyze the DSC experimental data. The temperature's measurement range was 20~600 °C, the heating rate was 5 °C/min, and the cooling rate was 10 °C/min.

The friction test was carried out using an MRH-3 high-speed "ring-on-block" wear tester with the ZSnSb11Cu6 sample as the lower sample and GCr15 steel rings (Ra 0.17–0.2 μm) as the upper sample. The test temperature of the friction and wear tests was room temperature, and the lubrication state was oil lubrication. The tests were conducted with a load of 250 N and a rotational speed of 500 r/min; the time of the tests was 30 min, and the lubricating oil used was 15W-40#. The experiment was carried out in an oil tank. The changes in friction coefficient, wear rate and wear morphology were observed by changing the content of the Y element. The same experiment was repeated three times, and the results were averaged, with the value of the coefficient of friction being the average of 30-min values. Before the test, each sample was cleaned by rough grinding, fine grinding and polishing to ensure that the surface roughness was Ra $\leq$ 0.8 μm and its quality was recorded. After wearing, washing with acetone and drying, the mass of each sample was weighed using a 1/10,000 electronic analytical balance, and its wear rate was calculated based on the weight of wear loss (average of multiple weighings). The morphology after wear was observed using a friction topography observer (HT-1000, Lanzhou Zhongke Kaihua Technology Development Co., Ltd., Lanzhou, China).

3. Results and Discussion

3.1. Mechanical Performance Analysis

The tensile strength, yield strength and elongation of all levels measured in the experiment are shown in Figure 1. Figure 2 shows the stress–strain curve.

Based on the experimental results, the tensile strength and yield strength of ZSnSb11Cu6 alloy were higher when no Y element was added. After adding a certain amount of Y, the tensile strength and yield strength of the modified ZSnSb11Cu6 alloy were greatly reduced, while the elongation rate increased rapidly. When the addition amount was 0.08%, the reduction in tensile strength was the smallest, decreasing from 100.4 MPa to 46.1 MPa, and the elongation rate increased from 2.25% to 43.5%. It can be concluded that the tensile strength and yield strength of the rare-earth alloy decreased while the elongation rate increased greatly. For alloy materials, their ductility needs to be improved to ensure the mechanical properties of the alloy. In this study, when 0.08 wt.% of the Y element was added, and the comprehensive performance of ZSnSb11Cu6 alloy was the best at this amount. If only the tensile strength of the alloy was considered, the addition of rare-earth Y decreased this property rather than increased it.

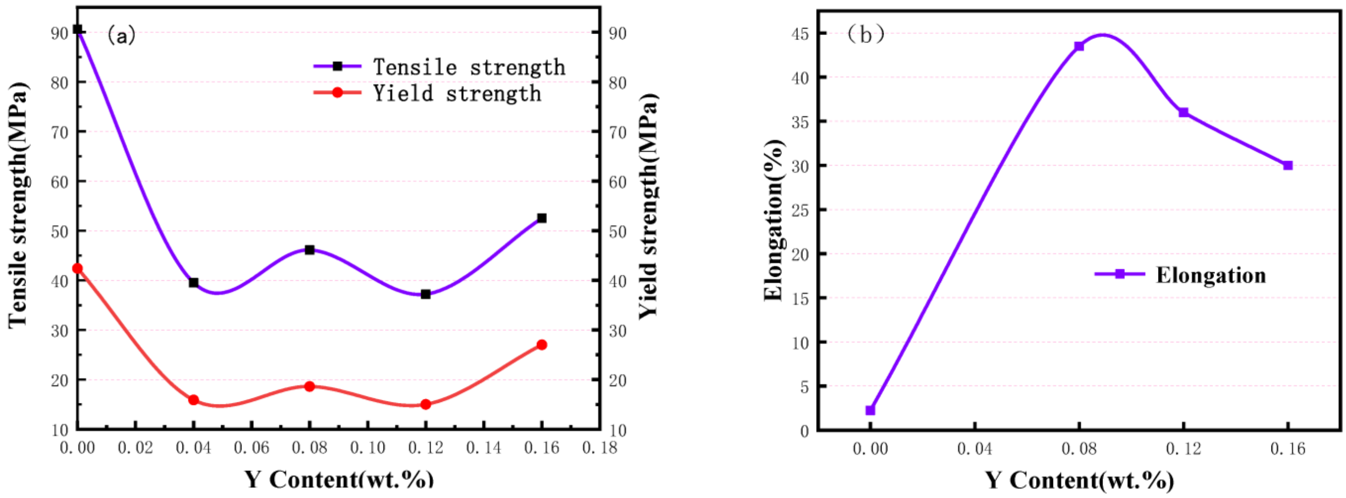

Figure 1. The tensile strength, yield strength (**a**) and elongation (**b**) of all levels measured.

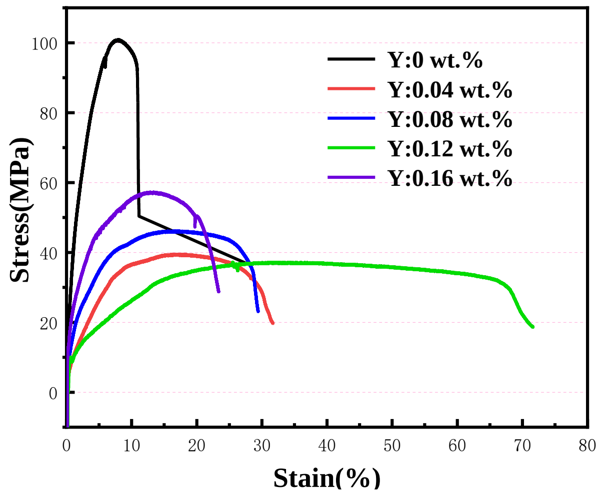

Figure 2. The stress-strain curve.

3.2. Observation and Analysis of Alloy Metallographic Organization

3.2.1. The Metallographic Organization

Figure 3 shows the metallographic organization of ZSnSb11Cu6 alloy with different rare-earth Y contents after corrosion.

Figure 3a shows the tissue topography of ZSnSb11Cu6 alloy without rare-earth Y added. It can be seen that white block particles form the hard SnSb phase, the white needle tissue is the Cu_6Sn_5 phase, and the black matrix tissue is a tin-based solid solution that forms the β soft matrix phase. The SnSb phase is evenly distributed in the tissue, with a square block of about 30–50 microns in length.

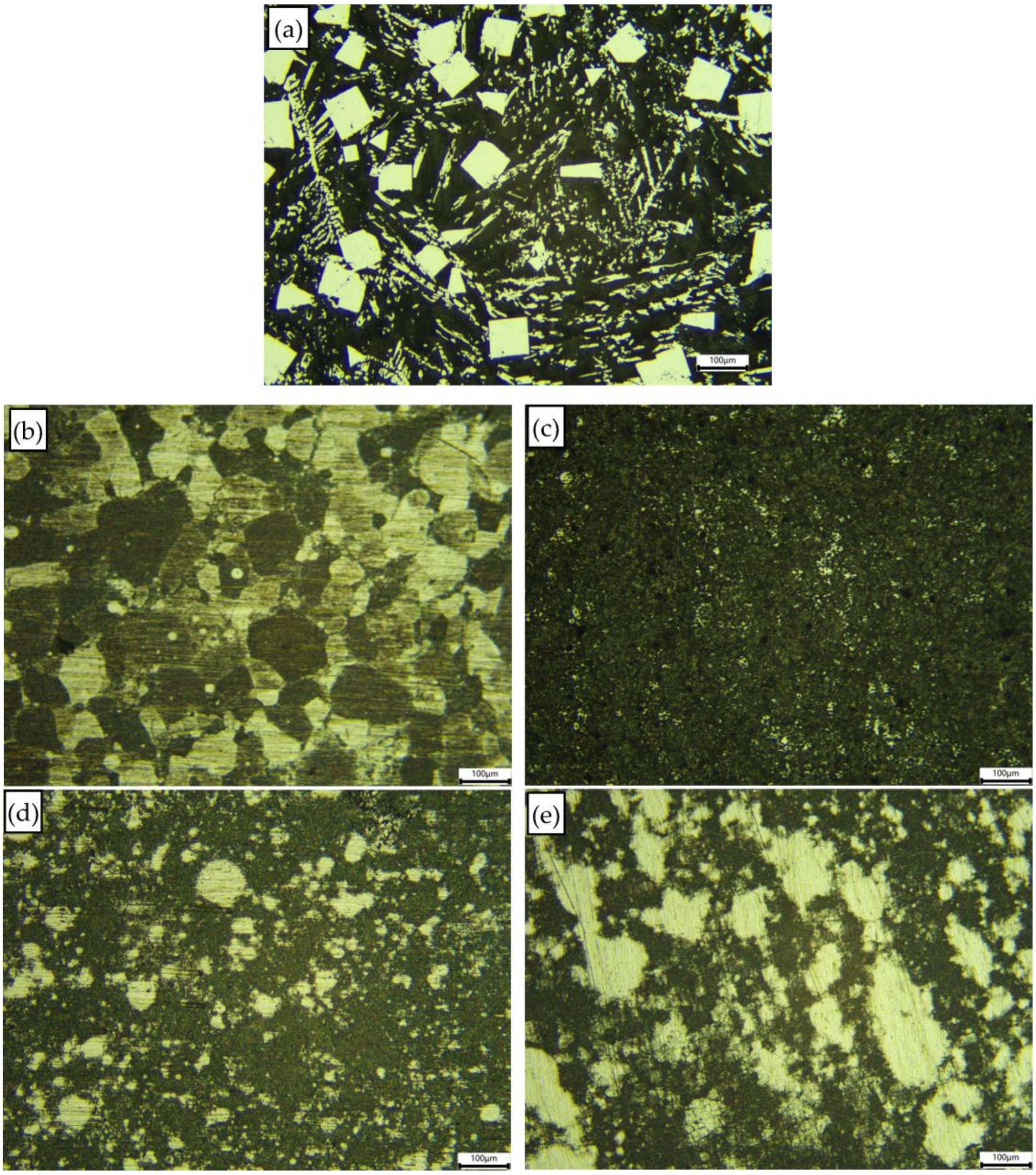

Figure 3. The metallographic organization after corrosion of ZSnSb11Cu6 alloy with different rare earth Y contents. (**a**) 0.0%; (**b**) 0.04%; (**c**) 0.08%; (**d**) 0.12%; (**e**) 0.16%.

As can be seen from Figure 3b–e, the quadratus SnSb particle phase was eliminated by the addition of rare-earth Y. In addition, the needle Cu_6Sn_5 phase also disappeared with the addition of Y, and the tissue changed from branch crystals to granular axial crystals. With an increase in the Y content, the grains became smaller, but they began to grow again with the continuous addition of the Y content. When the content of Y was 0.08 wt.%, the grains were the smallest.

3.2.2. EDS Analysis

EDS analysis of samples without Y and Y0.08 wt.%, as shown in Figure 4:

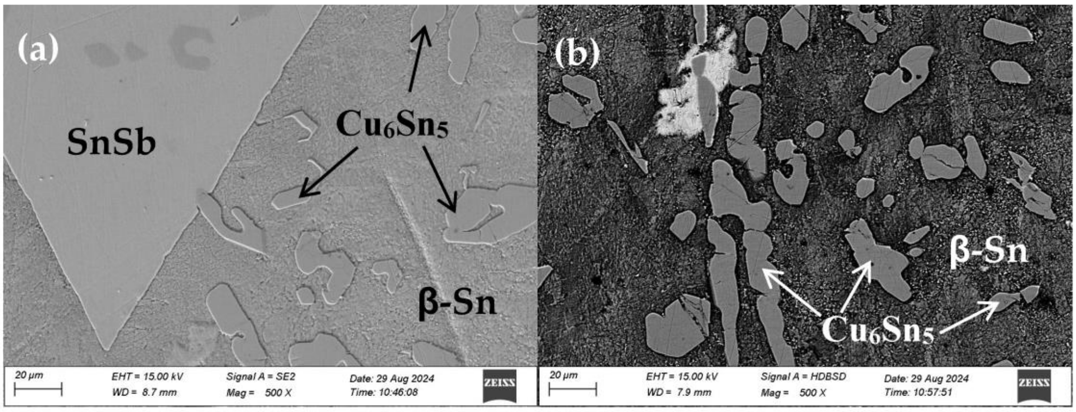

Figure 4. EDS of Y without addition and Y0.08 wt.%. (**a**) EDS analysis of samples without Y (**b**) EDS of Y0.08 wt.%.

Figure 4a shows the EDS data diagram of ZSnSb11Cu6 alloy without Y. Figure 4b shows the EDS data diagram of ZSnSb11Cu6 alloy with 0.08% Y. Face scan of these two tissues, as shown in Figures 5 and 6:

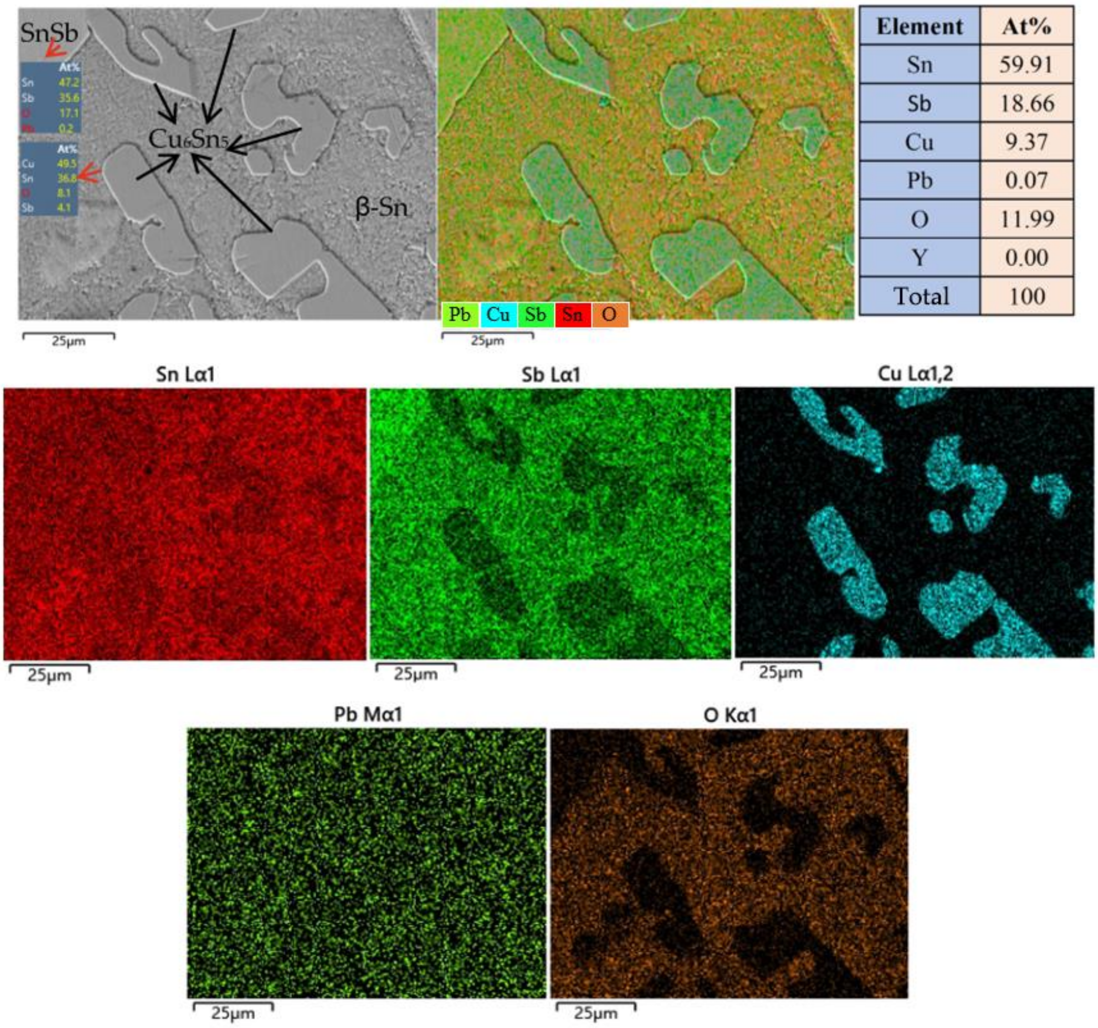

Element	At%
Sn	59.91
Sb	18.66
Cu	9.37
Pb	0.07
O	11.99
Y	0.00
Total	100

Figure 5. Distribution diagram of element of Y without addition. The Cu_6Sn_5 phase and SnSb phase are marked by black and red arrows respectively.

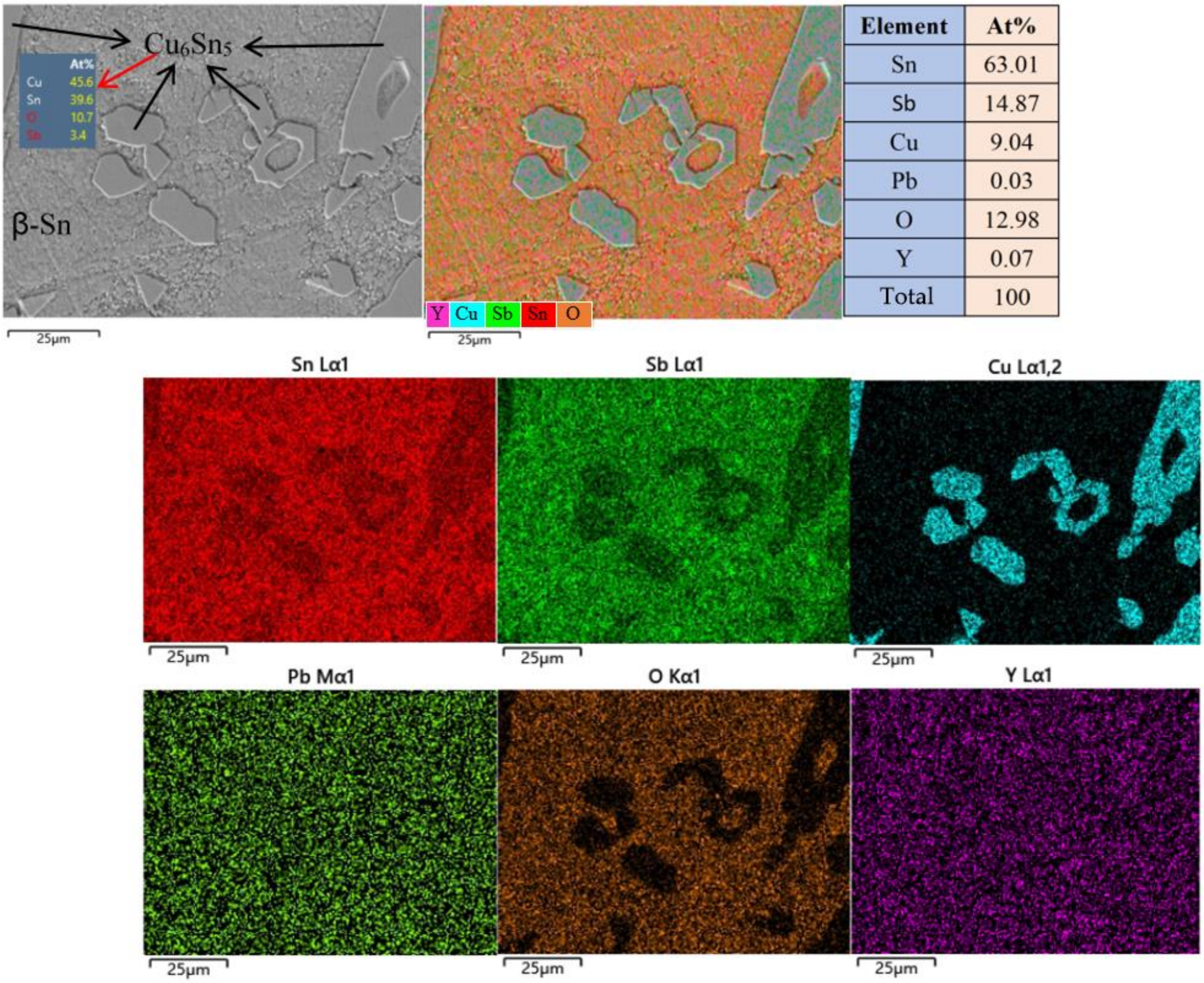

Figure 6. Distribution diagram of element of Y0.08 wt.%. The Cu_6Sn_5 phase is marked by black arrows, while the red arrow points to the corresponding EDS result.

As seen from the figure, the micro-organization of ZSnSb11Cu6 alloy without Y is mainly in the large bulk SnSb phase, the Cu_6Sn_5 phase, and the tin-based solid solution that forms the β soft matrix phase.

3.2.3. DSC Analysis

To determine whether the addition of Y had generated a new phase, the samples were analyzed under different heating conditions. The DSC curves for ZSnSb11Cu6 alloy with different Y contents are shown in Figure 7.

Figure 7a shows the relationship diagram of heat flow and temperature during the heating process of ZSnSb11Cu6 alloy with different rare-earth Y contents. From Figure 7, there is only one temperature transition point between 232 and 245 °C. As the melting point of tin is 231.89 °C, it can be concluded that the peak point is the melting temperature point of the ZSnSb11Cu6 alloy, and when rare-earth Y is not added, the melting point is 245.14 °C. Then, the melting temperature point and heat flow decrease as the Y content increases.

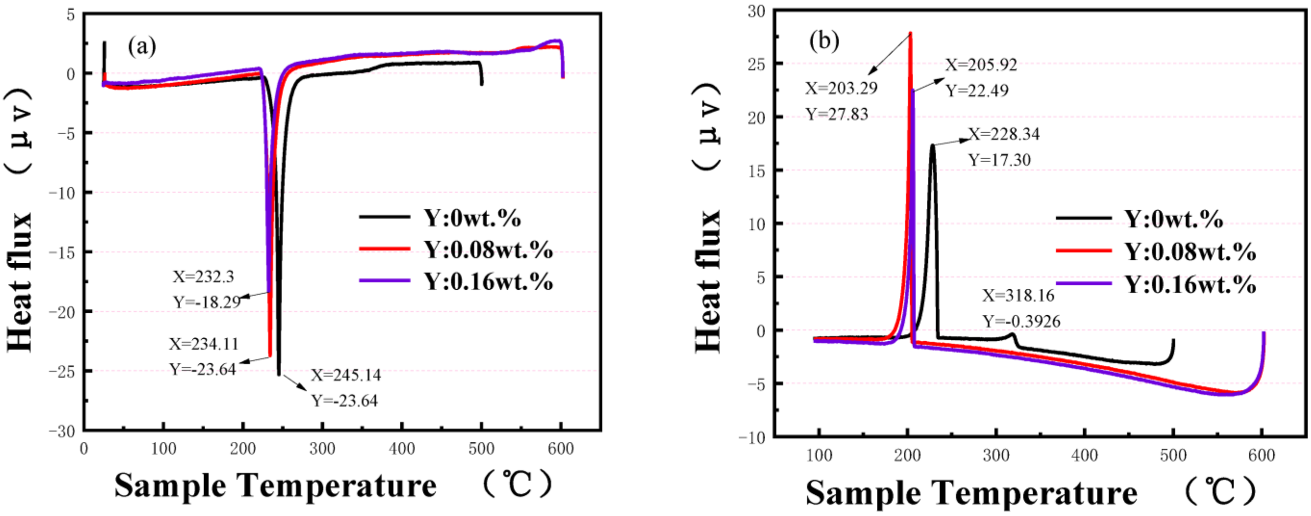

Figure 7. Temperature heat flow curves corresponding to different Y contents. (**a**) The warming process. (**b**) The cooling process.

Figure 7b shows the relationship between heat flow and temperature during the cooling process of ZSnSb11Cu6 alloy with different rare-earth Y contents. As can be seen from Figure 7b, during the cooling process, only a peak point appears between 203 and 205 °C. No new phases appear, and there are no precipitated peaks for the SnSb and Cu_6Sn_5 phases. According to the Sn-Sb binary phase diagram, the temperature point for the SnSb phase formation is 242 °C, and the melting point of Sb is 630 °C; thus, there is only a Sb-rich α phase in the organization. When no rare-earth Y is added, two peaks appear. The first strong peak is at about 228.34 °C, indicating the precipitation of the α phase. The second peak near 318 °C was initially judged to be the Cu_6Sn_5 hard phase, which did not appear after the addition of rare-earth Y. This conclusion is consistent with the results observed in the tissue topography. From the tissue perspective, the addition of Y has a great influence on the alloy tissue, and no SnSb particle phase was observed in the tissue.

3.3. Friction Coefficient

After sampling for friction and wear experiments, the friction coefficient of different rare earth Y was obtained as shown in Figure 8.

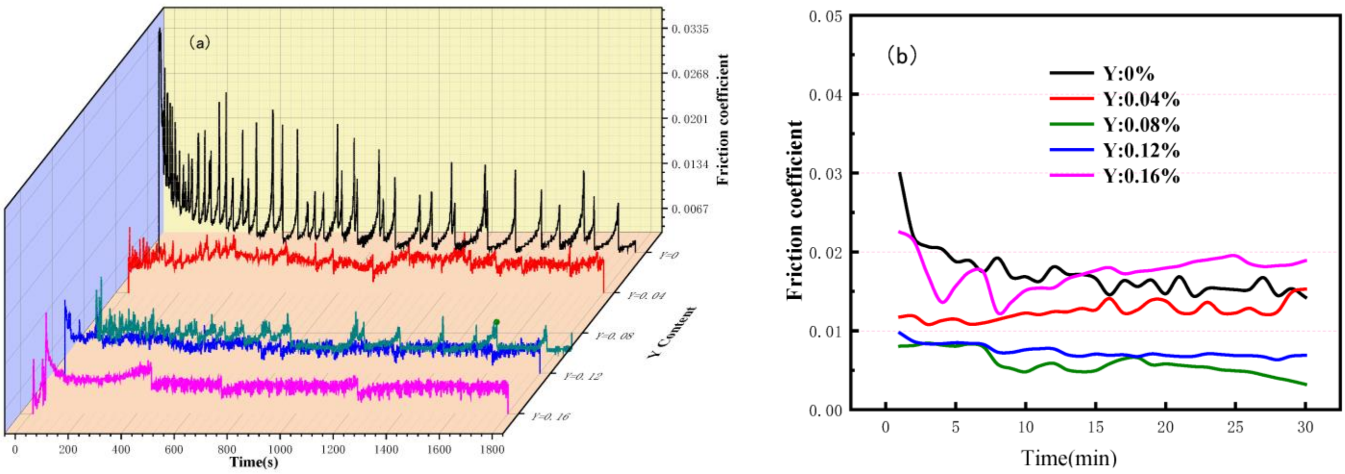

Figure 8. The friction coefficient of different rare earth Y was obtained. (**a**) The tested friction coefficient, (**b**) the friction coefficient plot of 30 mean points obtained from (**a**).

Figure 8a shows the plot of friction coefficient over time during the 30-min friction test under oil lubrication at a load of 250 N and a rotational speed of 500 r/min N after the addition of different contents of rare-earth Y. Figure 8b shows the friction coefficient plot of 30 mean points obtained from each set of rare-earth Y contents added to ZSnSb11Cu6 alloy.

It can be seen from the experimental data that after rare-earth Y was added, the friction coefficient was reduced. When rare-earth Y was not added, it can be seen from Figure 8a that the friction coefficient was not high and unstable, fluctuating greatly around 0.018. The reason for this is that there are more SnSb hard particles in the tissue. When the friction on the surface encounters the hard SnSb phase formed by large particles, it will affect the rotation of the friction ring, so the friction coefficient will fluctuate up and down.

However, after the addition of rare-earth Y, the large bulk SnSb phase in the tissue cannot be eliminated, so the overall friction coefficient is relatively low. With an increase in friction time, the overall fluctuation is relatively stable. As can be seen from Figure 8b, when the content of rare-earth Y was added to 0.08%, the friction coefficient was the smallest and fluctuated around 0.005. With a Y content of 0.08. and 0.12 wt.%, the friction coefficient was below 0.01, and when rare-earth Y was added to 0.04 wt.%, the friction coefficient fluctuated around 0.012. When the rare-earth Y content increased to 0.16 wt.%, the friction coefficient fluctuated around 0.015. These results show that with an increase in the rare-earth Y content, the friction coefficient first decreases and then increases. When the content exceeds 0.08%, the friction coefficient begins to increase. When the rare-earth Y content is 0.08%, the friction coefficient is minimum and fluctuates around 0.005.

The main reason is that the grains are significantly refined, and the needle Cu_6Sn_5 phase disappears as it evenly disperses into the tissue after adding rare-earth Y. The white massive particles in the hard β phase become particularly small particles, which are evenly distributed in the matrix and reduced in number. With an increase in the rare-earth Y content, the grains grow larger.

3.4. Wear Scar Morphology

The worn samples are selected for a 3D-grinding experiment, and the results are as follows:

The 3D profile of wear tracks on the sample under oil lubrication and subjected to a load of 250 N and a rotational speed of 500 r/min N is shown in Figure 9. The depth of the wear tracks decreases with the addition of Y. The grinding depth becomes shallow, and with an increase in the Y content, the grinding depth shows a trend of first decreasing and then increasing. When the addition of rare-earth Y was 0.08%, the grinding depth was the lowest. This trend of wear depth is consistent with the trend of friction coefficient of ZSnSb11Cu6 alloy with different contents of Y, and the surface of the wear tracks is smoother. The main reason is that with an increase in the Y content, the grains became smaller, but they began to grow again with the continuous addition of the Y content. When the content of Y was 0.08 wt.%, the grains were the smallest, and the large bulk SnSb phase could not be found in the tissue, while the friction coefficient was the minimum. Thus, when the addition of rare-earth Y was 0.08 wt.%, the grinding depth was the lowest.

As can be seen from the results of performance, the addition of rare-earth Y reduces the tensile strength and yield strength of ZSnSb11Cu6 alloy but greatly improves its elongation rate, indicating an increased plasticity. Moreover, no obvious cracks or severe adhesive wear were found on the alloy surface, indicating that large plastic deformation did not cause wear defects. On the contrary, the friction results indicate that small and uniform plastic deformation provides better wear resistance and fatigue strength. The finite plastic deformation caused by the addition of the Y element weakens the brittle fracture on the alloy surface layer caused by the Sb element by changing the dominant wear form.

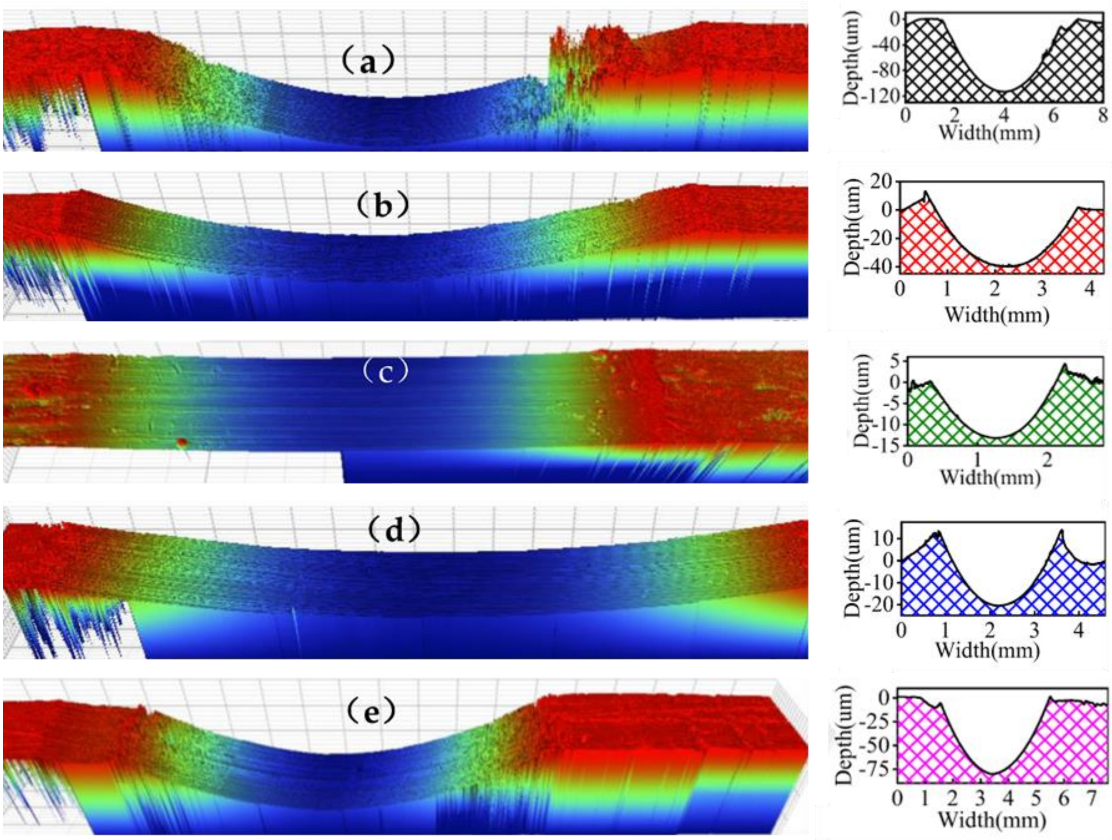

Figure 9. 3D morphology of partial wear surface and cross-sectional of partial wear tracks of (**a**) ZSnSb11Cu6Y0, (**b**) ZSnSb11Cu6Y0.04, (**c**) ZSnSb11Cu6Y0.08. (**d**) ZSnSb11Cu6Y0.12, (**e**) ZSnSb11Cu6Y0.16. Different colors indicate the height of different areas of the samples.

4. Conclusions

In this study, the microscopic structure, performance and tribological properties of ZSnSb11Cu6 alloy with different trace contents of rare-earth Y were investigated. A series of significant results were obtained, as follows:

(1) The addition of rare-earth Y greatly changed the organization of Sn–Babbitt alloy. The shape of the square SnSb phase and the needle Cu_6Sn_5 phase changed in the organization, and the tissue changed from dendritic crystals to granular equiaxial crystals. With an increase in the Y content, the grains first decreased and then increased in size. The grain size was smallest when the rare-earth Y content was 0.08 wt.%.

(2) When adding a certain content of Y, the tensile strength and yield strength of the modified ZSnSb11Cu6 alloy were greatly reduced, while the elongation rate increased rapidly. When the addition amount was 0.08%, the reduction in tensile strength was the smallest, decreasing from 100.4 MPa to 46.1 MPa, and the elongation rate increased from 2.25% to 43.5%.

(3) With an increase in the content of rare-earth Y, the friction coefficient first decreased and then increased. When the rare-earth Y content exceeded 0.08%, the friction coefficient began to increase. When the rare-earth Y content was 0.08%, the friction coefficient was the minimum and fluctuated around 0.005.

(4) The depth of the wear tracks decreased with the addition of the Y content. The grinding depth became shallow, and with an increase in the Y content, the grinding depth showed a trend of first decreasing and then increasing. When the addition of rare-earth Y was 0.08%, the grinding depth was the lowest.

Considering the above results, it can be seen that the addition of rare-earth Y reduces the tensile strength of the alloy but greatly improves its ductility as well as its friction and wear performance. These results show that rare-earth Y plays a role in improving the wear resistance of alloys.

Author Contributions: Writing, X.R.; data collection, Y.C.; the friction experiment, S.C.; the pouring experiment, N.C.; performance testing, Z.S.; the tissue morphology testing, Y.Z.; figures, H.C.; data analysis, Z.G.; data interpretation, G.Z.; literature search, J.H.; study design, H.X. All authors have read and agreed to the published version of the manuscript.

Funding: This project was supported by Fundamental Research Program of Shanxi Province (202403021211058), Fundamental Research Program of Shanxi Province (202303021211158), Fundamental Research Program of Shanxi Province (202103021224193) and Supported by the Opening Project of Shanxi Key Laboratory of Controlled Metal Solidification and Precision Manufacturing, North University of China, No. MSPM202004.

Institutional Review Board Statement: Not applicable.

Informed Consent Statement: Informed consent was obtained from all subjects involved in the study.

Data Availability Statement: Data are contained within the article.

Conflicts of Interest: The authors declare no conflict of interest.

References

1. Kamal, M.; El-Bediwi, A.; Lashin, A.R.; El-Zarka, A.H. Copper effects in mechanical properties of rapidly solidified Sn–Pb–Sb Babbitt bearing alloys. *Mat. Sci. Eng. A.* **2011**, *530*, 327–332. [CrossRef]
2. Zhang, X.Q.; Wu, S.H.; Liu, W.; Chu, X.; Xie, Y.; Zhang, F. High performance tin-based Babbitt coatings deposited by high-pressure cold spraying. *Surf. Coat. Technol.* **2023**, *473*, 130048. [CrossRef]
3. Xu, T.Z.; Zhang, S.; Wang, Z.; Zhang, C.; Zhang, D.; Wang, M.; Wu, C. Wear behavior of graphite self-lubricating Babbitt alloy composite coating on 20 steel prepared by laser cladding. *Eng. Fail. Anal.* **2022**, *141*, 106698. [CrossRef]
4. Zhou, F.M.; Li, J.; Xu, D.; Shi, M. Interface microstructure and properties of submerged arc brazing tin-based babbit. *China Weld.* **2019**, *28*, 45–49.
5. Ettles, C.M. Some factors affecting the design of spring supported thrust bearings in hydroelectric generators. *J. Tribol.* **1991**, *113*, 626–632. [CrossRef]
6. Iliev, H. Failure analysis of hydro-generator thrust bearing. *Wear* **1999**, *225*, 913–917. [CrossRef]
7. Kujawski, J.M.; Kitch, D.M.; Conway, L.E. The IRIS spool-type reactor coolant pump. In Proceedings of the 10th International Conference on Nuclear Engineering, Arlington, VA, USA, 14–18 April 2002; American Society of Mechanical Engineers: New York, NY, USA, 2002; pp. 999–1002.
8. Luo, W.R.; Lin, D.Y.; Xi, X.; Wang, Y.K.; Liu, Y.; Liu, D.; Chen, B.; Bian, H.; Song, Y.Y.; Liu, F.Y.; et al. High-strength and wear-resistant Babbitt alloy coatings prepared through in-situ alloying. *Surf. Coat. Technol.* **2024**, *494*, 131416. [CrossRef]
9. Ünlü, B.S.; Atik, E. Evaluation of effect of alloy elements in copper based Cu6Sn510 and CuZn30 bearings on tribological and mechanical properties. *J. Alloys Compd.* **2010**, *489*, 262–268. [CrossRef]
10. Fu, Y.C.; Wang, X. The Wear Mechanismof Babbit during Dry Sliding Friction. *Lubr. Eng.* **2011**, *36*, 32–34.
11. Yoo, Y.R.; Kim, Y.S. Influence of electrochemical properties on electrochemical migration of SnPb and SnBi solders. *Met. Mater. Int.* **2010**, *16*, 739–745. [CrossRef]
12. Zhou, Y.K.; Wang, Z.Y.; Zuo, X. Improving running-in quality of Babbitt alloy using h-BN as oil additives. *Wear* **2023**, *524–525*, 204807. [CrossRef]
13. Feyzullahoğlu, E.; Zeren, A.; Zeren, M. Tribological behaviour of tin-based materials and brass in oil lubricated conditions. *Mater. Des.* **2008**, *29*, 714–720. [CrossRef]
14. Tasgin, Y. The Effects of Boron Minerals on the Microstructure and Abrasion Resistance of Babbitt Metal (Sn–Sb–Cu) Used as Coating Materials in Hydroelectric Power Plants. *Int. J. Met.* **2020**, *14*, 257–265. [CrossRef]
15. Junior, P.R.C.A.; Pukasiewicz, A.G.M. Evaluation of microstructure, mechanical and tribological properties of a Babbitt alloy deposited by arc and flame spray processes. *Tribol. Int.* **2019**, *131*, 148–157. [CrossRef]
16. Nascimento, A.R.C.; Ettouil, F.B.; Moreau, C.; Savoie, S.; Schulz, R. Erratum to: Production of Babbitt Coatings by High Velocity Oxygen Fuel (HVOF) Spraying. *J. Therm. Spray Technol.* **2017**, *26*, 1741. [CrossRef]
17. Arab, S.M.; Zeidabadi, S.R.H.; Jahromi, S.A.J.; Daneshmanesh, H.; Zebarjad, S.M.; Janghorban, K. Fabrication of Al/Babbitt surface bearing through friction stir processing. *Ind. Lubr. Tribol.* **2017**, *69*, 930–937. [CrossRef]
18. Amanov, A.; Ahn, B.; Lee, M.G.; Jeon, Y.; Pyun, Y.-S. Friction and Wear Reduction of Eccentric Journal Bearing Made of Sn-Based Babbitt for Ore Cone Crusher. *Materials* **2016**, *9*, 950. [CrossRef]
19. Zhang, D.Y.; Zhang, H.; Liguo, Q.I.N. Effect of surface texturing on tribological properties of Babbitt alloy. *J. Huazhong Univ. Sci. Technol.* **2014**, *42*, 30.

20. Zhang, D.; Ho, J.K.L.; Dong, G.; Zhang, H.; Hua, M. Tribological properties of tin-based Babbitt bearing alloy with polyurethane coating under dry and starved lubrication conditions. *Tribol. Int.* **2015**, *90*, 22–31. [CrossRef]
21. Ji, X.; Chen, Y. Tribological behavior of Babbitt alloy rubbing against Si3N4, and steel under dry friction condition. *J. Mater. Eng. Perform.* **2016**, *25*, 750–755. [CrossRef]
22. Wu, H.; Bi, Q.; Zhu, S.; Yang, J.; Liu, W. Friction and wear properties of Babbitt alloy 16-16-2 under sea water environment. *Tribol. Int.* **2011**, *44*, 1161–1167. [CrossRef]
23. Wu, H.R.; Bi, Q.L.; Yang, J.; Liu, W.M. Tribological Performance of Tin-based White Metal ZChSnSb8-8 under Simulated Sea Water Environment. *Tribology* **2011**, *31*, 271–277.
24. Sürül, K.; Beiss, P.; Akin, O. Bindefestigkeit der Gleitlagerlegierung Sn-12Sb-6Cu-1,8Bi. Bonding strength of the babbit alloy Sn-12Sb-6Cu-1.8Bi. *Mater. Und Werkst.* **2010**, *41*, 657–665. [CrossRef]
25. Abioye, T.; Zuhailawati, H.; Azlan, M.; Anasyida, A. Effects of SiC additions on the microstructure, compressive strength and wear resistance of Sn-Sb-Cu bearing alloy formed via powder metallurgy. *J. Mater. Res. Technol.* **2020**, *9*, 13196–13205. [CrossRef]
26. Wang, J.L.; Wang, D.P.; Wang, X.H. Property improvement of tin-based BabbittB83 based on metallography control. *Mater. Sci. Technol.* **2018**, *26*, 89–96.
27. Cheng, Z.; Dong, X.; Zhang, Y.H.; Wang, M.; Long, W.M.; Zhu, T.; Zhang, L.; Zhou, J.F.; Wang, X.H. Effect of Ag, Co and Cr on Microstructure and Bonding Property of tin-based BabbittAlloy. *Electr. Weld. Mach.* **2023**, *53*, 113–118.
28. Gong, L.K.; Liao, J.F.; Yuan, J.H.; Li, G.; Chen, H. Effect of Rare Earth Y on Microstructure and Properties of Sn-58Bi Solder Alloy. *J. Aeronaut. Mater.* **2018**, *38*, 101–108.
29. Ren, X.Y.; Zhang, G.W.; Hong, X.; Sun, F.E. Study on microstructure control and performance optimization of ZCuPb20Sn5 alloy by rare earth la. *J. Phys. Conf. Ser.* **2020**, *1507*, 042006. [CrossRef]
30. Wang, Z.; Zhang, G.; Kang, Y.; Liu, Y.; Ren, X. The Effect of Y on the Microstructure, Mechanical and Wear Properties of ZCuSn10Pb10 Alloy. *Materials* **2022**, *15*, 1047. [CrossRef]